Modeling of tethered satellite formations using graph theory

Larsen, Martin Birkelund; Smith, Roy S; Blanke, Mogens

Published in:
Acta Astronautica

Link to article, DOI:
10.1016/j.actaastro.2011.05.014

Publication date:
2011

Acta Astronautica ▮ (▮▮▮▮) ▮▮▮–▮▮▮

Contents lists available at ScienceDirect

Acta Astronautica

journal homepage: www.elsevier.com/locate/actaastro

Modeling of tethered satellite formations using graph theory

Martin B. Larsen [a], Roy S. Smith [b,d], Mogens Blanke [a,c,*]

[a] Department of Electrical Engineering, Technical University of Denmark, Kgs. Lyngby, Denmark
[b] Department of Electrical and Computer Engineering, University of California, Santa Barbara, USA
[c] CeSOS, Norwegian University of Technology and Science, Trondheim, Norway
[d] Automatic Control Laboratory, Swiss Federal Institute of Technology (ETH), Zurich, Switzerland

ARTICLE INFO

Article history:
Received 14 June 2010
Received in revised form
8 May 2011
Accepted 16 May 2011

Keywords:
Tethered satellite formation
Graph theory
Equations of motion
Stationary configurations

ABSTRACT

Tethered satellite formations have recently gained increasing attention due to future mission proposals. Several different formations have been investigated for their dynamic properties and control schemes have been suggested. Formulating the equations of motion and investigation which geometries could form stable formations in space are cumbersome when done at a case to case basis, and a common framework providing a basic model of the dynamics of tethered satellite formations can therefore be advantageous. This paper suggests the use of graph theoretical quantities to describe a tethered satellite formation and proposes a method to deduce the equations of motion for the attitude dynamics of the formation in a compact form. The use of graph theory and Lagrange mechanics together allows a broad class of formations to be described using the same framework. A method is stated for finding stationary configurations and an upper limit of their number is determined. The method is shown to be valid for general tethered satellite formations that form a tree structure.

1. Introduction

Tethered satellite formations have been proposed in several contexts, especially in relation to remote sensing and space stations [1]. Several potential applications have been investigated in the literature. An elevator system for a space station using tethers was investigated in [2] and space elevators connecting Earth and space were suggested in [3]. Tether systems were proposed as atmospheric probes in [4], for interferometer missions [5], for space webs [6], and tethers are being considered for solar sail electric propulsion [7]. The dynamic properties and analysis of stability are essential for these applications.

Chain structures were studied by [8,9], ring structures were investigated by [10], hub-and-spoke structures by [11,12]. Anchored structures, also refereed to as double pyramid formations, were analysed in [13,11]. Ref. [11] suggested formations referred to as hub-and-spoke, which consist of a main satellite and a number of sub-satellites tethered to the main one. Closed-hub-and-spoke, where the sub-satellites are connected to each other, was also studied. The fact that not all topologies are stable was illustrated by the finding in [11] that interconnecting the sub-satellites in the hub-and-spoke structure turned out unstable and an anchor satellite was needed to obtain a stable topology. Significant effort have hence been given the study of specific structures, and a more generalized framework could be advantageous taking the number of proposed structures into account.

The chain structure is the kind of formation that has received the greatest attention. Chain topologies with a small number of satellites, three or four, were studied in

* Corresponding author at: Department of Electrical Engineering, Technical University of Denmark, Kgs. Lyngby, Denmark.
Tel.: +45 45352565; fax: +45 45881295.
E-mail addresses: martin_b_larsen@hotmail.com (M.B. Larsen), rsmith@control.ee.ethz.ch (R.S. Smith), mb@elektro.dtu.dk (M. Blanke).

0094-5765/$ - see front matter © 2011 Elsevier Ltd. All rights reserved.
doi:10.1016/j.actaastro.2011.05.014

[14,15], and [8,9] extended the analysis to general N-body chains. The simplest case of a chain topology is the one with two tethered satellites. The research on this problem is very mature and it is not in the scope of this article to give an overview of this field. For N-body chain structures, the equations of motion were deduced in [8] for in-plane and out-of-plane dynamics, and a simple relation was found between the natural frequency of in-plane and out-of-plane motions. The model was expanded in [16] to consider a varying tether length, flexibility of the tether and a non-circular orbit. The stationary configurations situated in the orbit plane of an N-body chain were found in [9] through an investigation of the stationary points of the potential energy and an upper limit on total number of stationary points was determined. The investigation was further expanded in [17] to also include the out-of-plane dimension of the configuration space. Another approach to determine stationary configurations of satellite formations was made in [18] where the equations of a stationary configuration were deduced assuming that two satellites of the formation could affect each other by a radial force. The general results on modeling of N-body TSS chains and assessment of which topologies would be stable, are essential for mission studies. Similar results are therefore needed for more general topologies.

This work considers tethered satellite formations forming a tree structure, i.e. a structure without cycles. Generic modeling, which is cumbersome with present methods, is made significantly simpler by employing graph theoretical quantities to describe tether formation and combine these with the Lagrange formalism to formulate generic equations of motion. This is shown to lead to a dynamic model where topology is parametrized through a path matrix that describes the topology. The equations of motion are deduced for a formation with constant-length tethers using the path matrix as parameter. The dynamics is derived for motion in the orbit plane as well as generally for motion in three dimensions. The dynamic equations for an N-body formation are well known for chain structures [8] and the contribution of this work is the generalization to tree structures, which is obtain by parameterizing the dynamics through the topology graph. This paper also includes a method to determine the stationary configurations of N-body trees in the orbit plane. The stationary configurations have previously been investigated for chain structures [9], but the generalization to tree structures is a novel contribution of the present paper.

The outline of the remaining part of the article is as follows. Means for a topology description of the tethered satellite formation are introduced in Section 2. Section 3 treats the derivation of the equations of motion for the motion in the orbit plane. Stationary configurations in the orbit plane are dealt with in Section 4 where a method for finding all such configurations is stated and the configurations are classified according to the number of vertical tethers in a configuration. Section 5 uses a Y-formation with four tethers to exemplify the investigation of stationary configurations. Section 6 offers conclusions of the work.

2. Formation topology description

Consider a tethered satellite formation consisting of massless tethers connecting satellites in a tree structure. The limitation to a tree structure is introduced to simplify the equations of motion by avoiding algebraic constraints associated with cycles within a formation. In a tree structure with $n+1$ satellites there are n tethers, with each tether connecting two satellites. Each satellite is modeled as a point mass m_i for $i=0,\ldots,n$ and tethers are modeled as rigid rods of constant length l_j for $j=1,\ldots,n$. The total mass of the system is denoted $m=\sum_{i=0}^{n} m_i$ and the relative mass of each satellite is $\mu_i=m_i/m$ for $i=0,\ldots,n$. The relative masses and the length of the rods are collected in the diagonal matrices $\boldsymbol{\Lambda}\in\mathbb{R}^{(n+1)\times(n+1)}$, $\boldsymbol{\Lambda}=\mathrm{diag}(\mu_0,\mu_1,\ldots,\mu_n)$, and $\boldsymbol{L}\in\mathbb{R}^{n\times n}$, $\boldsymbol{L}=\mathrm{diag}(l_1,l_2,\ldots,l_n)$. The formation is described by a connected, directed graph representing masses as nodes and rods as edges. The notation m_i and l_j is reused to denote the nodes and the edges of the graph. The graph forms a rooted tree where the node m_0 represents the root. The root of the tree can be chosen arbitrarily. It is assumed, without loss of generality that each edge is directed away from the root and that the edge l_k is connected to and directed towards m_k. The formation topology can then be described by the incidence matrix $\boldsymbol{B}\in\mathbb{R}^{(n+1)\times n}$ where each row represents a node and each column an edge. The incidence matrix $\boldsymbol{B}$ with elements B_{ij} is defined as

$$B_{ij}=\begin{cases}1 & \text{if } l_j \text{ is connected to and pointing away from } m_i,\\ -1 & \text{if } l_j \text{ is connected to and pointing towards } m_i,\\ 0 & \text{if } l_j \text{ is not connected to } m_i.\end{cases} \tag{1}$$

With the assumption of a tree structure, the incidence matrix $\boldsymbol{B}$ has full rank and by removing one row from $\boldsymbol{B}$ a square matrix of full rank is formed. This square matrix is called the basic incidence matrix or the reduced incidence matrix with respect to the node corresponding to the removed row. The basic incidence matrix $\boldsymbol{A}\in\mathbb{R}^{n\times n}$ describes the structure with respect to the root that is the sub-matrix of $\boldsymbol{B}$ which excludes the first row. The path from a node m_i to the root is unique and can be described as a column of the path matrix $\boldsymbol{P}\in\mathbb{R}^{n\times n}$. The ith column represents the directed path from m_i to m_0 such that,

$$P_{ji}=\begin{cases}1 & \text{if } l_j \text{ is in the path from } m_i \text{ to } m_0 \text{ directed towards } m_0,\\ -1 & \text{if } l_j \text{ is in the path from } m_i \text{ to } m_0 \text{ directed towards } m_i,\\ 0 & \text{if } l_j \text{ is not in the path from } m_i \text{ to } m_0.\end{cases} \tag{2}$$

All non-zero elements of $\boldsymbol{P}$ are negative due to the definition of the direction of the edges. The basic incidence matrix and the path matrix are related as each others inverse

$$\boldsymbol{P}=\boldsymbol{A}^{-1}, \tag{3}$$

according to [19, Theorem 2.10, pp. 55–56].

Please cite this article as: M.B. Larsen, et al., Modeling of tethered satellite formations using graph theory, Acta Astronautica (2011), doi:10.1016/j.actaastro.2011.05.014

Some sets connected to the graph are introduced in the following. These sets are used in connection with the determination of the stationary configuration of the formation. The set T_j comprise the nodes in a sub-tree rooted at m_j. The sub-tree occurs when the graph is divided into two disjoint connected graphs by removing the edge l_j. After introducing T_j, the path matrix can be written as

$$P_{ji} = \begin{cases} -1 & \text{for } i \in T_j, \\ 0 & \text{for } i \notin T_j. \end{cases} \tag{4}$$

Definition (2) is valid for a tree structure with arbitrary directed edges, while (4) is only valid assuming edges are directed away from the root.

The set J includes an arbitrary combination of edges. The set can be decomposed into sets J_k for $k = 1, \ldots, \ell$ each describing a connected structure. It is assumed that the elements of the set J_k are not connected to elements in J_p for $k \neq p$, this means the decomposition is minimal in the sense that ℓ is as small as possible. The complement of the set J is denoted $\bar{J}$ and the cardinality of these sets are denoted $|J|$ and $|\bar{J}|$, respectively. The set of neighboring edges of l_j is denoted N_j, meaning that the edge l_k is included in N_j if one of the two nodes incident with l_j is also incident with l_k. The notation $N_J = (\bigcup_{i \in J} N_i) \backslash J$ is used for the neighboring edges of J. The notation is illustrated by an example in Appendix A.

3. Equations of motion

The equations of the attitude motion of the satellite formation are derived in this section. The derivation follows the derivation in [8], but takes the general tree structure into account. To describe the attitude motion of the formation the orbit frame is introduced. The frame is centered at the center of mass (CM) of the formation and has the x-axis along the position vector from the Earth to the CM and the z-axis perpendicular to the orbit plane. The masses of the formation are described by a position vector $\boldsymbol{r}_i = [x_i \; y_i \; z_i]^T$ for $i = 0, \ldots, n$ and a vector along the positive direction of each rod is introduced as $\boldsymbol{\rho}_j = [\xi_j \; \eta_j \; \zeta_j]^T$ for $j = 1, \ldots, n$ (see Fig. 1). Using the path matrix, the position of m_i for $i = 1 \ldots n$ can be found relative to m_0. To be able to describe the position of all masses, including m_0, by a single expression, the path matrix is expanded to $\tilde{\boldsymbol{P}} \in \mathbb{R}^{n \times (n+1)}$ such that $\tilde{\boldsymbol{P}} = [\boldsymbol{0}_n \; \boldsymbol{P}]$. The additional column of zeros $\boldsymbol{0}_n \in \mathbb{R}^n$ can be interpreted as representing the path from the root node to itself. This path does not contain any edges. Using $\tilde{\boldsymbol{P}}$ the position vector of each mass can be written as a sum along the path to the mass

$$\boldsymbol{r}_i = \boldsymbol{r}_0 - \sum_{j=1}^{n} \tilde{P}_{j(i+1)} \boldsymbol{\rho}_j \quad \text{for } i = 0, \ldots, n. \tag{5}$$

The sign of the sum originates from the fact that the vectors $\boldsymbol{\rho}_j$ are pointing away from the root, while the paths are directed towards the root. Since the frame is centered at the CM, the position vectors obey the relation $\sum_i m_i \boldsymbol{r}_i = 0$, which combined with (5) leads to the position vector of m_0

$$\boldsymbol{r}_0 = \sum_{j=1}^{n} \boldsymbol{\rho}_j \sum_{k=1}^{n} \tilde{P}_{j(k+1)} \mu_k. \tag{6}$$

Substituting (5) back into (6) the position vectors of the masses in the formation are

$$\begin{aligned} \boldsymbol{r}_i &= -\sum_{j=1}^{n} \left(\tilde{P}_{j(i+1)} - \sum_{k=1}^{n} \tilde{P}_{j(k+1)} \mu_k \right) \boldsymbol{\rho}_j \\ &= \sum_{j=1}^{n} \left(\sum_{k=1}^{n} \tilde{P}_{j(k+1)} (\mu_k - \delta_{ik}) \right) \boldsymbol{\rho}_j, \end{aligned} \tag{7}$$

where δ_{ik} is Kronecker's delta. Eq. (7) gives the relation between the position of m_i and the directions of the rods l_j. By collecting x_i in a vector $\boldsymbol{x} \in \mathbb{R}^{n+1}$ and ξ_j in a vector $\boldsymbol{\xi} \in \mathbb{R}^n$ defined as

$$\boldsymbol{x} = [x_0 \; x_1 \; \ldots \; x_n]^T, \tag{8}$$

$$\boldsymbol{\xi} = [\xi_1 \; \xi_2 \; \ldots \; \xi_n]^T, \tag{9}$$

the relation of the x-component of (7) can be written in the compact form

$$\boldsymbol{x} = \boldsymbol{\Gamma} \boldsymbol{P}^T \boldsymbol{\xi}. \tag{10}$$

The components of the matrix $\boldsymbol{\Gamma} \in \mathbb{R}^{(n+1) \times n}$ are given as

$$\Gamma_{ik} = \mu_k - \delta_{i(k+1)}. \tag{11}$$

Introducing $\boldsymbol{y}, \boldsymbol{z} \in \mathbb{R}^{n+1}$ similar to $\boldsymbol{x}$ and $\boldsymbol{\eta}, \boldsymbol{\zeta} \in \mathbb{R}^n$ similar to $\boldsymbol{\xi}$, the relations can be expanded to the position along the y- and z-axis as

$$\boldsymbol{y} = \boldsymbol{\Gamma} \boldsymbol{P}^T \boldsymbol{\eta}, \tag{12a}$$

$$\boldsymbol{z} = \boldsymbol{\Gamma} \boldsymbol{P}^T \boldsymbol{\zeta}. \tag{12b}$$

Note that the original path matrix $\boldsymbol{P}$ is used in this relation, not the expanded version $\tilde{\boldsymbol{P}}$.

In the following, the equations of motion are derived under the assumption of constant length rods and a CM following a circular orbit with orbital rate ω. For simplicity, we first restrict the derivation of the dynamics of this formation to the motion in the orbit plane. The derivation for the general three dimensional motion is included in Appendix B. Due to the assumption of a circular orbit, ω is constant, and the true anomaly $v = \omega t$ is introduced as the time variable for the system. The in-plane angles θ_j are chosen as generalized coordinates and are collected in the vector $\boldsymbol{\theta} = [\theta_1, \ldots, \theta_n]^T$. The in-plane angle θ_j is defined

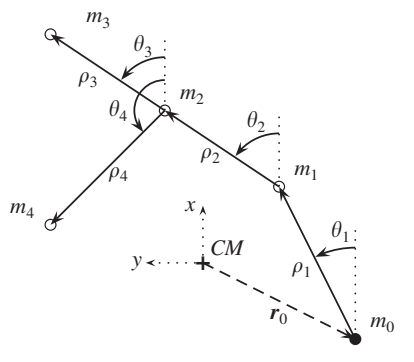

Fig. 1. A tethered satellite formation in the orbit plane.

Please cite this article as: M.B. Larsen, et al., Modeling of tethered satellite formations using graph theory, Acta Astronautica (2011), doi:10.1016/j.actaastro.2011.05.014

with respect to axes parallel with the orbit frame centered at the initial node of l_j, as seen in Fig. 1. The vectors along the rods are then

$$\boldsymbol{\rho}_j = \begin{bmatrix} l_j \cos\theta_j \\ l_j \sin\theta_j \end{bmatrix}. \tag{13}$$

The velocity of each mass in the inertial frame can be written as $\boldsymbol{V}_i = \boldsymbol{V}_{CM} + \boldsymbol{v}_i$ for $i = 0, \ldots, n$, where $\boldsymbol{V}_{CM}$ is the velocity of the CM and $\boldsymbol{v}_i$ is the velocity of m_i relative to the CM. The relative velocity is

$$\boldsymbol{v}_i = \begin{bmatrix} \omega \dot{x}_i - \omega y_i \\ \omega \dot{y}_i + \omega x_i \end{bmatrix}, \tag{14}$$

where $(\dot{\ })$ denotes the first derivative with respect to v relative to the orbit frame. The total kinetic energy of the formation can be written as

$$\mathcal{T} = \frac{m}{2} |\boldsymbol{V}_{CM}|^2 + \sum_{i=0}^{n} m_i \boldsymbol{V}_{CM} \cdot \boldsymbol{v}_i + \frac{1}{2} \sum_{i=0}^{n} m_i |\boldsymbol{v}_i|^2. \tag{15}$$

Only the last term of (15) contributes to the equations of motion, since the first term is constant and the second term vanishes in Lagrange's equation. With an assumption that the length of each rod l_j is much smaller than the orbit radius, the potential energy of the system can be approximated by

$$\mathcal{V} = \mathcal{V}_{CM} + \frac{\omega^2}{2} \sum_{i=0}^{n} m_i (|\boldsymbol{r}_i|^2 - 3x_i^2), \tag{16}$$

where $\mathcal{V}_{CM}$ is the constant orbital energy of the circular orbit, which will not contribute to the attitude motion. From the energy functions the equations of motion can be found using Lagrange's equation

$$\frac{d}{dv} \frac{\partial \mathcal{T}}{\partial \dot{\theta}_j} - \frac{\partial \mathcal{T}}{\partial \theta_j} + \frac{\partial \mathcal{V}}{\partial \theta_j} = 0, \quad j = 1, \ldots, n. \tag{17}$$

Inserting (15) and (16) in (17) results in the equations of motion

$$\mathcal{M} \ddot{\boldsymbol{\theta}} + \mathcal{G} = 0, \tag{18}$$

where

$$\mathcal{M} = \boldsymbol{E}_{\sin\theta} \boldsymbol{LGLE}_{\sin\theta} + \boldsymbol{E}_{\cos\theta} \boldsymbol{LGLE}_{\cos\theta}, \tag{19a}$$

$$\mathcal{G} = (\boldsymbol{E}_{\sin\theta} \boldsymbol{LGLE}_{\cos\theta} - \boldsymbol{E}_{\cos\theta} \boldsymbol{LGLE}_{\sin\theta})(2\boldsymbol{I} + \boldsymbol{E}_{\dot{\theta}}) \dot{\theta} + 3 \boldsymbol{E}_{\sin\theta} \boldsymbol{LGLE}_{\cos\theta} \boldsymbol{1}_n. \tag{19b}$$

The matrices $\boldsymbol{E}_{\cos\theta} \in \mathbb{R}^{n \times n}$ and $\boldsymbol{E}_{\sin\theta} \in \mathbb{R}^{n \times n}$ are diagonal matrices with $\cos\theta_j$ and $\sin\theta_j$, respectively, at the jth diagonal entry. Similarly $\boldsymbol{E}_{\dot{\theta}} \in \mathbb{R}^{n \times n}$ is diagonal with $\dot{\theta}_j$ at the jth diagonal entry. All elements of the vector $\boldsymbol{1}_n \in \mathbb{R}^n$ equal 1. All parameters of the model are then collected in a single matrix $\boldsymbol{LGL}$ where

$$\boldsymbol{G} = \boldsymbol{P\Gamma}^T \boldsymbol{\Lambda \Gamma P}^T. \tag{20}$$

Here $\boldsymbol{G} \in \mathbb{R}^{n \times n}$ is referred to as the mass matrix of the system. The mass matrix will be investigated further in the next section, in connection with determination of stationary configurations of the system.

4. Stationary configuration in the orbit plane

In this section, the stationary configurations of the system are investigated. We restrict the investigation to the stationary configuration in the orbit plane. The in-plane stationary configuration can be treated separately, since the motion in the orbit plane is restricted to an invariant manifold in state space (see Appendix B). It should, however, be emphasized that stationary configurations exist, which are not situated in the orbit plane. In [17] these general stationary configurations have been investigated for a chain structure. The present investigation follows the same steps as [9] and is based on the same properties but are extended to the present case of a tree structure, making use of the graph-based parameterisation of the topology.

4.1. Properties of mass matrix

For the analysis of the stationary configuration the mass matrix $\boldsymbol{G}$ is of significant importance. We therefore start this section by stating some properties regarding $\boldsymbol{G}$, which will be used when finding and analyzing the stationary configuration of the formation. Proofs of the properties of this section can be found in Appendix C. From (20) the matrix $\boldsymbol{W} \in \mathbb{R}^{n \times n}$ is defined as $\boldsymbol{W} = \boldsymbol{\Gamma}^T \boldsymbol{\Lambda \Gamma}$ such that the mass matrix can be written as

$$\boldsymbol{G} = \boldsymbol{PWP}^T. \tag{21}$$

From the definition of $\boldsymbol{\Gamma}$ in (11) the elements of $\boldsymbol{W}$ can be found as

$$W_{ik} = \mu_i \delta_{ik} - \mu_i \mu_k. \tag{22}$$

The matrix $\boldsymbol{W}$ is clearly symmetric and obeys the following property.

Property 1. *The matrix $\boldsymbol{W}$ is positive definite and the elements of the inverse matrix are given as,*

$$W_{ki}^{-1} = \frac{1}{\mu_0} + \frac{\delta_{ki}}{\mu_i}. \tag{23}$$

Property 1 serves mainly to prove the statements regarding $\boldsymbol{G}$ in the next property.

Property 2. *The mass matrix $\boldsymbol{G}$ is symmetric and positive definite. The elements of its inverse satisfies the property that $G_{jk}^{-1} = 0$ for $k \notin N_j \wedge j \neq k$.*

The last point in Property 2 states that the transformation of $\boldsymbol{G}$ into an identity matrix can be made by linear combinations consisting only of columns corresponding to neighboring edges. This point is similar to Property 1 in [9]. The assumption $k \notin N_j$ is equivalent to $j \notin N_k$, which must be the case since $\boldsymbol{G}$ is symmetric.

The elements of $\boldsymbol{G}$ can be formulated by means of the sub-trees T_j of the graph introduced in Section 2. This formulation is useful when proving Property 3 and it will be treated further in the proof of that property. First the sum M_{jk} is introduced as

$$M_{jk} = \sum_{i \in T_j \cap T_k} \mu_i. \tag{24}$$

Please cite this article as: M.B. Larsen, et al., Modeling of tethered satellite formations using graph theory, Acta Astronautica (2011), doi:10.1016/j.actaastro.2011.05.014

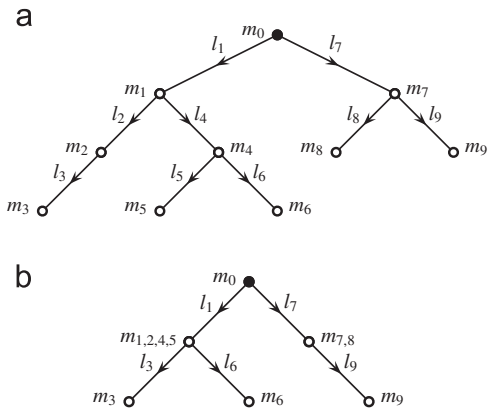

Fig. 2. Graph and its by $J=\{2, 4, 5, 8\}$ reduced counterpart: (a) original graph and (b) reduced graph.

The definition is based on the nodes of two arbitrary sub-trees in the graph, T_j and T_k. The sum is taken over the intersection of the two trees, hence for M_{jk} to be different from zero T_j must be a sub-tree in T_k or vice versa. Using M_{jk} the elements for $\boldsymbol{G}$ can be written as

$$G_{jk} = M_{jk} - M_{jj}M_{kk}. \tag{25}$$

Note that M_{jj} sums the nodes in the sub-tree T_j and is therefore always different from zero.

When solving the equation leading to the stationary configuration a reduced version of the mass matrix will occur. From an arbitrary set of rods J with complement $\bar{J}$ the reduced mass matrix $\widehat{\boldsymbol{G}} \in \mathbb{R}^{|\bar{J}|\times|\bar{J}|}$ is defined by removing the rows and columns corresponding to rods in the set J. We connect a reduced graph with the set J. The graph occurs when the edges in the set J are removed from the graph as shown in Fig. 2. The reduction is done based on the decomposition of $J=\bigcup_k J_k$ introduced in Section 2. Each component J_k forms a tree. The tree J_k can be assumed rooted at a node m_i if all edges $j \in J_k$ are included in sub-tree T_i. The mass m_i is denoted the root of J_k. The sub-tree T_i can be decomposed into J_k and a number of sub-trees. When the tree J_k is removed from the graph, these sub-trees are connected to the root of J_k. The following property, which is illustrated in Fig. 2, shows a relation between the graph reduced by the set J and the reduced matrix $\widehat{\boldsymbol{G}}$.

Property 3. *Consider a graph reduced by the set $J=\bigcup_k J_k$ and the roots m_i of J_k. Assume that the nodes m_i are assigned the sum of the nodes in the sub-trees J_k, while the remaining nodes stay unchanged. Then the mass matrix of the reduced graph will equal the reduced mass matrix $\widehat{\boldsymbol{G}}$ of the original graph.*

The important point regarding Property 3 is that $\widehat{\boldsymbol{G}}$ is the mass matrix for a different graph, hence the statement in Property 2 also applies to $\widehat{\boldsymbol{G}}$. When working with the reduced graph we keep referring to the rods according to the original graph. This also applies when referring to rows, columns, and elements of the corresponding matrices and vectors.

The next property addresses the similarity between $\widehat{\boldsymbol{G}}^{-1}$ and $\boldsymbol{G}^{-1}$.

Property 4. *Assume that $j,k \in \bar{J}$ such that the element $\widehat{\boldsymbol{G}}^{-1}_{jk}$ exists, then*

$$\widehat{G}^{-1}_{jk} = G^{-1}_{jk} \quad \text{for } j,k \notin N_J. \tag{26}$$

This property states that the common elements of a row of $\widehat{\boldsymbol{G}}^{-1}$ representing an edge with no neighbors in J is unchanged compared to $\boldsymbol{G}^{-1}$, hence the reduction only introduces a local change in the inverse mass matrix. Furthermore, using Property 2 it can be seen that the elements excluded from the row compared to $\boldsymbol{G}^{-1}$ in this case equal zero. Note that $\widehat{\boldsymbol{G}}^{-1}$ is symmetric, hence the property could just as well be explained with respect to columns.

4.2. Equation of stationary configuration

From the equations of motion (18) a stationary configuration $\boldsymbol{\theta}^*$ in the orbit plane is found as a solution to the equation

$$\boldsymbol{E}^*_{\sin\theta}\boldsymbol{G}\boldsymbol{\xi}^* = \boldsymbol{0}_n, \tag{27}$$

where $\boldsymbol{\xi}^* = [l_1 \cos\theta^*_1, \ldots, l_n \cos\theta^*_n]^T$ and $\boldsymbol{E}^*_{\sin\theta}$ denotes $\boldsymbol{E}_{\sin\theta}$ evaluated at $\boldsymbol{\theta}=\boldsymbol{\theta}^*$. The first thing to note about (27) is that the stationary configurations are symmetric in the sense that if $\boldsymbol{\theta}^*$ is a stationary configuration so is $\overline{\boldsymbol{\theta}}^* = \pi\boldsymbol{1}_n - \boldsymbol{\theta}^*$. In a stationary configuration a rod is characterized as horizontal if $\cos\theta^*_k = 0$. If $\sin\theta^*_k = 0$ the rod is vertical. Eq. (27) is in general solved by choosing a set J containing vertical rods, hence $\sin\theta^*_j = 0$ for $j \in J$. Denoting the rows of $\boldsymbol{G}$ as $\boldsymbol{G}_j$ for $j=1,\ldots,n$, the matrix Eq. (27) can be divided into n coupled scalar equations

$$\sin\theta^*_j \boldsymbol{G}_j^T \boldsymbol{\xi}^* = 0 \quad \text{for } j=1,\ldots,n. \tag{28}$$

From (28) it is seen that for each vertical rod one of the n equations is solved, hence introducing J leaves $|\bar{J}|$ equations to be solved.

Two choices of J stand out from the general solution procedure. First $J=\emptyset$ where no rods are situated in a vertical position. In this case (27) reduces to

$$\boldsymbol{G}\boldsymbol{\xi}^* = \boldsymbol{0}_n. \tag{29}$$

Due to Property 2 the equation has a unique solution $\boldsymbol{\xi}^* = \boldsymbol{0}_n$ corresponding to rods situated in a horizontal position. Each rod can have two different orientations in a horizontal position (corresponding to symmetric configurations), hence there are 2^n different configurations for $\boldsymbol{\xi}^* = \boldsymbol{0}_n$. The second special case is $\bar{J}=\emptyset$, i.e. all rods are in a vertical position. In this case, all n equations in (28) are solved immediately. A rod in a vertical position has two different orientations, which again leads to 2^n configurations. The existence of the 2^{n+1} configurations in the two special cases are independent of the parameters of the system. These stationary configurations are similar to the four stationary configurations induced by the gravity gradient for a single rod in orbit.

Please cite this article as: M.B. Larsen, et al., Modeling of tethered satellite formations using graph theory, Acta Astronautica (2011), doi:10.1016/j.actaastro.2011.05.014

In the remaining cases where $J \neq \emptyset$ and $\bar{J} \neq \emptyset$ Eq. (27) can be written as

$$\widehat{\boldsymbol{G}}\hat{\boldsymbol{\xi}}^* = -\sum_{k\in J} \hat{\boldsymbol{g}}_k \xi_k^*, \tag{30}$$

where $\hat{\boldsymbol{\xi}}^*$ equals $\boldsymbol{\xi}^*$ reduced by the set J. The vector $\hat{\boldsymbol{g}}_k$ is the kth column of $\boldsymbol{G}$ reduced by the elements in J. Note that $\hat{\boldsymbol{g}}_k$ does not equal the kth column of the reduced mass matrix $\widehat{\boldsymbol{G}}$ since $k \in J$. Eq. (30) gives the relation between the rods fixed in a vertical position ξ_k^* for $k \in J$ and the orientation of the remaining rods are collected in $\hat{\boldsymbol{\xi}}^*$. The vertical orientation implies that $\xi_k^* = \pm l_k$ for $k \in J$, hence (30) actually includes $2^{|J|}$ equations taking all sign combinations into account. According to Property 3 the matrix $\widehat{G}$ has full rank, and the solution of (30) is unique for each right-hand side. The existence of each configuration can be investigated from the vector $\hat{\boldsymbol{\sigma}} \in \mathbb{R}^{|\bar{J}|}$,

$$\hat{\boldsymbol{\sigma}} = -\widehat{\boldsymbol{L}}^{-1}\widehat{\boldsymbol{G}}^{-1}\sum_{k\in J} \hat{\boldsymbol{g}}_k \xi_k^*, \tag{31}$$

where $\widehat{\boldsymbol{L}}$ is a reduced version of $\boldsymbol{L}$. The elements of $\hat{\boldsymbol{\sigma}}$ equal $\hat{\sigma}_j = \cos\theta_j^*$ for $j \in \bar{J}$. Hence the stationary configuration exists if the absolute value of all elements of $\hat{\boldsymbol{\sigma}}$ are less than one, $|\hat{\sigma}_j| < 1$ for $j \in \bar{J}$. Note that the case $|\hat{\sigma}_j| = 1$ is not included, since this would contradict the assumption that $j \in \bar{J}$.

The similarity between $\boldsymbol{G}^{-1}$ and $\widehat{\boldsymbol{G}}^{-1}$ stated in Property 4 can be used together with the knowledge of the zero elements of $\boldsymbol{G}^{-1}$ from Property 2 to conclude that,

$$(\widehat{\boldsymbol{G}}_j^{-1})^T \hat{\boldsymbol{g}}_k = 0 \quad \text{for } k \in J,\ j \notin N_J, \tag{32}$$

where $\widehat{\boldsymbol{G}}_j^{-1}$ denotes the jth column of $\widehat{\boldsymbol{G}}^{-1}$. From (31) it is seen that this implies that $\hat{\sigma}_j = 0$ if $j \notin N_J$. The geometrical interpretation of this property is that, in a stationary configuration, only the neighbors of a vertical rod will be affected, while all others will remain horizontal. Hence it can be concluded that the stationary configuration consists of groups of either horizontal or vertical rods, which are separated by no more than one inclined rod. This was also concluded in [9] for a chain structure. The vertical groups are orthogonal to the horizontal groups and therefore no forces can be transferred along the inclined rods, in stationary configurations. This furthermore shows that all horizontal groups are placed along the y-axis where the centrifugal force cancels the gravitational force. A detailed stability analysis of the configurations is not in the scope of this article, but the above description indicates that all formation with one or more horizontal groups will be unstable, since the masses of these groups will balance at the unstable equilibrium between the centrifugal and the gravitational force.

Since both $\boldsymbol{G}$ and $\widehat{\boldsymbol{G}}$ have full rank, the described method will result in all possible stationary configurations of the system. The total number of possible stationary configurations can be found by realizing that the set J can be chosen in 2^n different ways. Each rod have two possible orientations, hence there are $2^{|J|}2^{|\bar{J}|} = 2^n$ possible orientations for each choice of J. This leads to a total number of possible configurations of 2^{2n}. This limit is the same as was obtained for a chain structure in [9].

5. Example

This example will consider five satellites and four tethers in a Y-formation as illustrated in Fig. 3. The nodes m_0 and m_2 are marked to better illustrate the formation. This is also done in the Figs. 4–6. The incidence matrix of the Y-formation is given as

$$\boldsymbol{B} = \begin{bmatrix} 1 & 0 & 0 & 0 \\ -1 & 1 & 0 & 0 \\ 0 & -1 & 1 & 1 \\ 0 & 0 & -1 & 0 \\ 0 & 0 & 0 & -1 \end{bmatrix}. \tag{33}$$

Using this incidence matrix and (21) the mass matrix is

$$\boldsymbol{G} = \begin{bmatrix} \mu_0(1-\mu_0) & \mu_0\mu_{2,3,4} & \mu_0\mu_3 & \mu_0\mu_4 \\ \mu_0\mu_{2,3,4} & (1-\mu_0-\mu_1)\mu_{2,3,4} & (1-\mu_0-\mu_1)\mu_3 & (1-\mu_0-\mu_1)\mu_4 \\ \mu_0\mu_3 & (1-\mu_0-\mu_1)\mu_3 & (1-\mu_3)\mu_3 & -\mu_3\mu_4 \\ \mu_0\mu_4 & (1-\mu_0-\mu_1)\mu_4 & -\mu_3\mu_4 & (1-\mu_4)\mu_4 \end{bmatrix}, \tag{34}$$

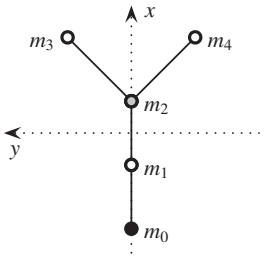

Fig. 3. Y-formation.

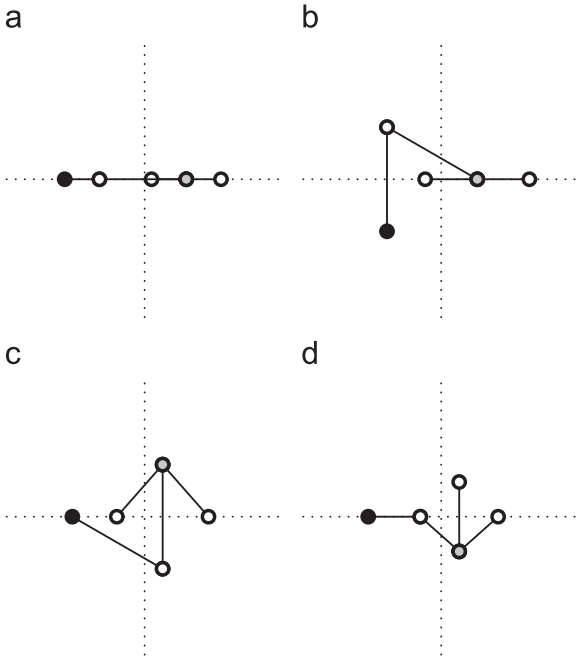

Fig. 4. Y-formations with $|J| = 0$ or $|J| = 1$: (a) $J = \emptyset$, (b) $J = \{1\}$, (c) $J = \{2\}$, and (d) $J = \{3\}, \{4\}$.

Please cite this article as: M.B. Larsen, et al., Modeling of tethered satellite formations using graph theory, Acta Astronautica (2011), doi:10.1016/j.actaastro.2011.05.014

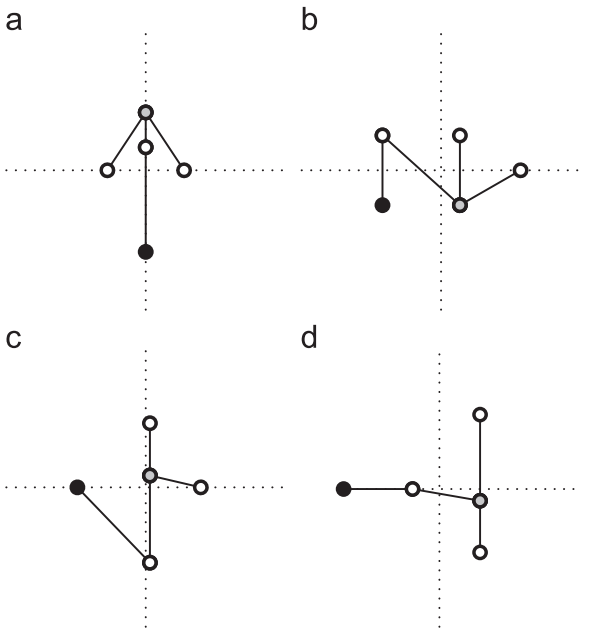

Fig. 5. Y-formations with $|J|=2$: (a) $J=\{1, 2\}$, (b) $J=\{1, 3\}$, $\{1, 4\}$, (c) $J=\{2, 3\}$, $\{2, 4\}$, and (d) $J=\{3, 4\}$.

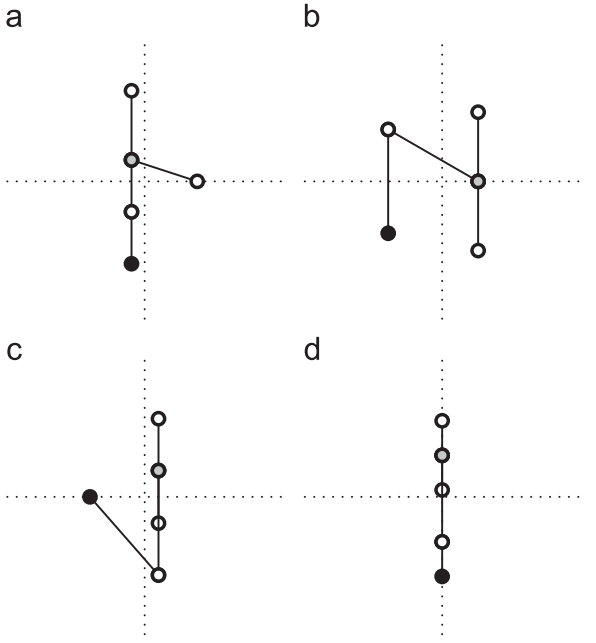

Fig. 6. Y-formations with $|J|=3$ or $|J|=4$: (a) $J=\{1, 2, 3\}$, $\{1, 2, 4\}$, (b) $J=\{1, 3, 4\}$, (c) $J=\{2, 3, 4\}$, and (d) $J=\{1, 2, 3, 4\}$.

where $\mu_{2,3,4}=\mu_2+\mu_3+\mu_4$. The inverse is given as

$$\boldsymbol{G}^{-1}=\begin{bmatrix} \frac{\mu_0+\mu_1}{\mu_0\mu_1} & -\frac{1}{\mu_1} & 0 & 0 \\ -\frac{1}{\mu_1} & \frac{\mu_1+\mu_2}{\mu_1\mu_2} & -\frac{1}{\mu_2} & -\frac{1}{\mu_2} \\ 0 & -\frac{1}{\mu_2} & \frac{\mu_2+\mu_3}{\mu_2\mu_3} & \frac{1}{\mu_2} \\ 0 & -\frac{1}{\mu_2} & \frac{1}{\mu_2} & \frac{\mu_2+\mu_4}{\mu_2\mu_4} \end{bmatrix}. \tag{35}$$

According to the previous section, the total number of possible stationary configurations is 256 for this example. The qualitatively different configurations are illustrated in Figs. 4–6. The configurations are found by fixing the masses uniformly and adjusting the length of the rods to illustrate the formation best possible and ensure that a stationary configuration actually exists. It is emphasized that the figures only exemplify configurations, since for each choice of J, there exist 16 configurations divided into 8 symmetric pairs. The formations illustrate that a horizontal rod only affects its neighboring rods, while the remaining rods will maintain their vertical orientation. It is also seen that masses not connected to a rod in the set J are placed along the y-axis. Examining the configurations it is seen that rods that are neither vertical nor horizontal, and are connected to a group at both ends, separating two groups of either horizontal or vertical rods. Such rods cannot affect either of the groups with forces, since the configuration is stationary.

6. Conclusions

With the aim of easing the task of modeling dynamics of tethered satellite formations, and determine stationary configurations, this paper combined graph theory with Lagrange formalism to obtain a generic framework for modeling. Imposing an assumption of a tree structure on the formation, enabled the path between the satellites, along the tethers, to be unique. Furthermore it allowed the paths from sub-satellites to a main satellite to be described by a single matrix quantity. A generic method for modeling was obtained by using this path matrix together with Lagrange formalism and the equations of motion were derived for both the in-plane motion and for the general three dimensional case. Constant-length rigid tethers and a circular orbit were assumed for the formation. The assumption of a tree structure simplified the equations, since the absence of algebraic constraints around cycles in the formation resulted in a formulation where each tether represents a single degree of freedom. A particular feature of the methodology was that the equations of motion were given in a matrix formulation, with the desirable property that all physical parameters, as well as the formation description, were captured by a single matrix. Furthermore, a method of finding the stationary configurations in the orbit plane was suggested, using the generic equations of motion. These configurations were classified based on the numbers of rods situated in a vertical equilibrium position and the upper limit of stationary configurations was determined to be the same as that of a chain structure. The method could be expanded to take stationary configurations into account that were not situated in the orbit plane. This would complicate the method and an upper limit would need be established for this case. The main advantage of the modeling based on graph theory presented in this article is that a broad class of formation can be treated collectively, and that both dynamic and stationary properties can be dealt with through this formalism.

Please cite this article as: M.B. Larsen, et al., Modeling of tethered satellite formations using graph theory, Acta Astronautica (2011), doi:10.1016/j.actaastro.2011.05.014

Appendix A. Example of notation

This appendix contain a short example of the notation used in connection with the description of the satellites formation. The formation with ten satellites and nine tethers shown in Fig. A.1 is used to illustrate notation. The corresponding incidence matrix and path matrix are

$$\boldsymbol{B}=\begin{bmatrix} 1 & 0 & 0 & 0 & 0 & 0 & 1 & 0 & 0\\ -1 & 1 & 0 & 1 & 0 & 0 & 0 & 0 & 0\\ 0 & -1 & 1 & 0 & 0 & 0 & 0 & 0 & 0\\ 0 & 0 & -1 & 0 & 0 & 0 & 0 & 0 & 0\\ 0 & 0 & 0 & -1 & 1 & 1 & 0 & 0 & 0\\ 0 & 0 & 0 & 0 & -1 & 0 & 0 & 0 & 0\\ 0 & 0 & 0 & 0 & 0 & -1 & 0 & 0 & 0\\ 0 & 0 & 0 & 0 & 0 & 0 & -1 & 1 & 1\\ 0 & 0 & 0 & 0 & 0 & 0 & 0 & -1 & 0\\ 0 & 0 & 0 & 0 & 0 & 0 & 0 & 0 & -1 \end{bmatrix}, \tag{A.1}$$

$$\boldsymbol{P}=\begin{bmatrix} -1 & -1 & -1 & -1 & -1 & -1 & 0 & 0 & 0\\ 0 & -1 & -1 & 0 & 0 & 0 & 0 & 0 & 0\\ 0 & 0 & -1 & 0 & 0 & 0 & 0 & 0 & 0\\ 0 & 0 & 0 & -1 & -1 & -1 & 0 & 0 & 0\\ 0 & 0 & 0 & 0 & -1 & 0 & 0 & 0 & 0\\ 0 & 0 & 0 & 0 & 0 & -1 & 0 & 0 & 0\\ 0 & 0 & 0 & 0 & 0 & 0 & -1 & -1 & -1\\ 0 & 0 & 0 & 0 & 0 & 0 & 0 & -1 & 0\\ 0 & 0 & 0 & 0 & 0 & 0 & 0 & 0 & -1 \end{bmatrix}. \tag{A.2}$$

Some of the sets introduced are listed in Table A.1 for the graph of the example in Fig. A.1.

Appendix B. Equations of motion in three dimensions

A two degree of freedom model taking both in-plane and out-of-plane motion into account is deduced in this appendix. The procedure is identical to the one used for the in-plane motion in Section 3, but the derivation becomes more cumbersome due to the additional states and the interaction between in-plane and out-of-plane motions. Denoting the out-of-plane angle φ, the vectors along the rods can be written as

$$\boldsymbol{\rho}_j=\begin{bmatrix} l_j\cos\theta_j\cos\varphi_j\\ l_j\sin\theta_j\cos\varphi_j\\ l_j\sin\varphi_j \end{bmatrix}. \tag{B.1}$$

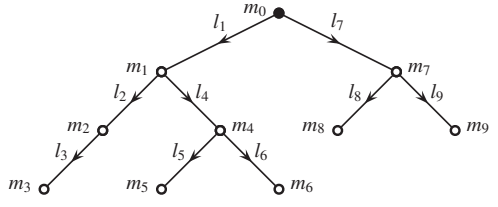

Fig. A.1. Graph of a rooted tree.

Table A.1
Definition of sets occurring in the graph in Fig. A.1.

(a) sets regarding edges		
	N_j	T_j
$j=1$	{2, 4, 7}	{1, 2, 3, 4, 5, 6}
$j=4$	{1, 2, 5, 6}	{4, 5, 6}
$j=9$	{7, 8}	{9}

(b) sets regarding the set J		
	N_J	J_k
J={2, 4, 5, 8}	{1, 3, 6, 7, 9}	{2, 4, 5}, {8}
J={1, 7, 9}	{2, 4, 8}	{1, 7, 9}
J={3, 5, 6}	{2, 4}	{3}, {5, 6}

The relative velocity of the mass m_i is expanded with an out-of-plane component, compared to (14)

$$\boldsymbol{v}_i=\begin{bmatrix} \omega\dot{x}_i-\omega y_i\\ \omega\dot{y}_i+\omega x_i\\ \omega\dot{z}_i \end{bmatrix}. \tag{B.2}$$

The kinetic and the potential energies are unchanged compared to (15) and (16). Inserting the energies including the out-of-plane motion into Lagrange's equation, the system can be written as

$$\begin{bmatrix} \mathcal{M}_{11} & \mathcal{M}_{12}\\ \mathcal{M}_{12}^T & \mathcal{M}_{22} \end{bmatrix}\begin{bmatrix} \ddot{\boldsymbol{\theta}}\\ \ddot{\boldsymbol{\varphi}} \end{bmatrix}+\begin{bmatrix} \mathcal{G}_1\\ \mathcal{G}_2 \end{bmatrix}=0, \tag{B.3}$$

where the matrices can be found to be

$$\mathcal{M}_{11}=\boldsymbol{E}_{\sin\theta}\boldsymbol{E}_{\cos\varphi}\tilde{\boldsymbol{G}}\boldsymbol{E}_{\sin\theta}\boldsymbol{E}_{\cos\varphi}+\boldsymbol{E}_{\cos\theta}\boldsymbol{E}_{\cos\varphi}\tilde{\boldsymbol{G}}\boldsymbol{E}_{\cos\theta}\boldsymbol{E}_{\cos\varphi}, \tag{B.4a}$$

$$\begin{aligned}\mathcal{M}_{22}=&\boldsymbol{E}_{\cos\theta}\boldsymbol{E}_{\sin\varphi}\tilde{\boldsymbol{G}}\boldsymbol{E}_{\cos\theta}\boldsymbol{E}_{\sin\varphi}+\boldsymbol{E}_{\cos\varphi}\tilde{\boldsymbol{G}}\boldsymbol{E}_{\cos\varphi},\\ &+\boldsymbol{E}_{\sin\theta}\boldsymbol{E}_{\sin\varphi}\tilde{\boldsymbol{G}}\boldsymbol{E}_{\sin\theta}\boldsymbol{E}_{\sin\varphi}\end{aligned} \tag{B.4b}$$

$$\mathcal{M}_{12}=\boldsymbol{E}_{\sin\theta}\boldsymbol{E}_{\cos\varphi}\tilde{\boldsymbol{G}}\boldsymbol{E}_{\cos\theta}\boldsymbol{E}_{\sin\varphi}-\boldsymbol{E}_{\cos\theta}\boldsymbol{E}_{\cos\varphi}\tilde{\boldsymbol{G}}\boldsymbol{E}_{\sin\theta}\boldsymbol{E}_{\sin\varphi}, \tag{B.4c}$$

$$\begin{aligned}\mathcal{G}_1=&(\boldsymbol{E}_{\sin\theta}\boldsymbol{E}_{\cos\varphi}\tilde{\boldsymbol{G}}\boldsymbol{E}_{\cos\theta}\boldsymbol{E}_{\cos\varphi}-\boldsymbol{E}_{\cos\theta}\boldsymbol{E}_{\cos\varphi}\tilde{\boldsymbol{G}}\boldsymbol{E}_{\sin\theta}\boldsymbol{E}_{\cos\varphi})\\ &\times((2\boldsymbol{I}+\boldsymbol{E}_{\dot{\theta}})\dot{\boldsymbol{\theta}}+\boldsymbol{E}_{\dot{\varphi}}\dot{\boldsymbol{\varphi}})-2(\boldsymbol{E}_{\sin\theta}\boldsymbol{E}_{\cos\varphi}\tilde{\boldsymbol{G}}\boldsymbol{E}_{\sin\theta}\boldsymbol{E}_{\sin\varphi}\\ &+\boldsymbol{E}_{\cos\theta}\boldsymbol{E}_{\cos\varphi}\tilde{\boldsymbol{G}}\boldsymbol{E}_{\cos\theta}\boldsymbol{E}_{\sin\varphi})(\boldsymbol{I}+\boldsymbol{E}_{\dot{\theta}})\dot{\boldsymbol{\varphi}}\\ &+3\boldsymbol{E}_{\sin\theta}\boldsymbol{E}_{\cos\varphi}\tilde{\boldsymbol{G}}\boldsymbol{E}_{\cos\theta}\boldsymbol{E}_{\cos\varphi}\mathbf{1}_n,\end{aligned} \tag{B.4d}$$

$$\begin{aligned}\mathcal{G}_2=&(\boldsymbol{E}_{\cos\theta}\boldsymbol{E}_{\sin\varphi}\tilde{\boldsymbol{G}}\boldsymbol{E}_{\cos\theta}\boldsymbol{E}_{\cos\varphi}+\boldsymbol{E}_{\sin\theta}\boldsymbol{E}_{\sin\varphi}\tilde{\boldsymbol{G}}\boldsymbol{E}_{\sin\theta}\boldsymbol{E}_{\cos\varphi})\\ &\times((2\boldsymbol{I}+\boldsymbol{E}_{\dot{\theta}})\dot{\boldsymbol{\theta}}+\boldsymbol{E}_{\dot{\varphi}}\dot{\boldsymbol{\varphi}})-\boldsymbol{E}_{\cos\varphi}\tilde{\boldsymbol{G}}\boldsymbol{E}_{\sin\varphi}\boldsymbol{E}_{\dot{\varphi}}\dot{\boldsymbol{\varphi}}\\ &+2(\boldsymbol{E}_{\sin\theta}\boldsymbol{E}_{\sin\varphi}\tilde{\boldsymbol{G}}\boldsymbol{E}_{\cos\theta}\boldsymbol{E}_{\sin\varphi}\\ &-\boldsymbol{E}_{\cos\theta}\boldsymbol{E}_{\sin\varphi}\tilde{\boldsymbol{G}}\boldsymbol{E}_{\sin\theta}\boldsymbol{E}_{\sin\varphi})(\boldsymbol{I}+\boldsymbol{E}_{\dot{\theta}})\dot{\boldsymbol{\varphi}}\\ &+3\boldsymbol{E}_{\cos\theta}\boldsymbol{E}_{\sin\varphi}\tilde{\boldsymbol{G}}\boldsymbol{E}_{\cos\theta}\boldsymbol{E}_{\cos\varphi}\mathbf{1}_n+\boldsymbol{E}_{\cos\varphi}\tilde{\boldsymbol{G}}\boldsymbol{E}_{\sin\varphi}\mathbf{1}_n.\end{aligned} \tag{B.4e}$$

The matrices $\boldsymbol{E}_{\cos\varphi}$ and $\boldsymbol{E}_{\sin\varphi}$ are defined similarly to $\boldsymbol{E}_{\cos\theta}$ and $\boldsymbol{E}_{\sin\theta}$, while $\boldsymbol{E}_{\dot{\varphi}}$ is defined in the same way as $\boldsymbol{E}_{\dot{\theta}}$. All parameters are collected in the matrix $\tilde{\boldsymbol{G}}=\boldsymbol{LGL}$, in the same way as for the in-plane motion. The equations shows that motion in the orbit plane does not give rise to a motion out of the plane, hence the in-plane motion compose an invariant manifold. By contrast, the opposite is not the case. An out-of-plane motion will excite the in-plane dynamics.

Please cite this article as: M.B. Larsen, et al., Modeling of tethered satellite formations using graph theory, Acta Astronautica (2011), doi:10.1016/j.actaastro.2011.05.014

Appendix C. Proof of properties

Proof of Property 1. To prove that $\boldsymbol{W}$, $W_{ik}=\mu_i\delta_{ik}-\mu_i\mu_k$, is positive definite, it is used that $\boldsymbol{W}$ is symmetric. The Sylvester Criterion [20, 7.2.5, p. 404] states that a Hermitian is positive definite if the determinant of all upper left sub-matrices as well as the matrix itself are positive definite. First $\boldsymbol{W}$ is rewritten in the matrix form

$$\boldsymbol{W}=\tilde{\boldsymbol{\Lambda}}-\boldsymbol{\mu}\boldsymbol{\mu}^T, \tag{C.1}$$

where $\tilde{\boldsymbol{\Lambda}}\in\mathbb{R}^{n\times n}$ is a diagonal matrix $\tilde{\Lambda}_{ik}=\mu_i\delta_{ik}$ and $\boldsymbol{\mu}=[\mu_1\ \dots\ \mu_n]^T$. The matrix determinant lemma can be used to find the determinant of the sub-matrices. The upper left square matrices can be found by truncating $\tilde{\boldsymbol{\Lambda}}$ and $\boldsymbol{\mu}$. The truncated versions containing ℓ elements are denoted $\boldsymbol{W}_\ell,\tilde{\boldsymbol{\Lambda}}_\ell\in\mathbb{R}^{\ell\times\ell}$ and $\boldsymbol{\mu}_\ell\in\mathbb{R}^\ell$. The matrix determinant lemma states that $\det(\boldsymbol{A}+\boldsymbol{u}\boldsymbol{v}^T)=(1+\boldsymbol{v}^T\boldsymbol{A}^{-1}\boldsymbol{u})\det\boldsymbol{A}$, which, applied to the sub-matrices, leads to

$$\det\boldsymbol{W}_\ell=(1-\boldsymbol{\mu}_\ell\tilde{\boldsymbol{\Lambda}}_\ell^{-1}\boldsymbol{\mu}_\ell^T)\det\tilde{\boldsymbol{\Lambda}}_\ell=\left(\mu_0+\sum_{j=\ell+1}^{n}\mu_j\right)\prod_{j=1}^{\ell}\mu_j>0. \tag{C.2}$$

For $\ell=n$ the determinant of $\boldsymbol{W}$ is

$$\det\boldsymbol{W}=\prod_{i=0}^{n}\mu_i>0, \tag{C.3}$$

which means that $\boldsymbol{W}$ is positive definite. The inverse of $\boldsymbol{W}$ can be found from (C.1) using the Sherman–Morrison formula [20, 0.7.4, pp. 18–19]

$$\boldsymbol{W}^{-1}=\tilde{\boldsymbol{\Lambda}}^{-1}+\frac{\mathbf{1}_n\mathbf{1}_n^T}{\mu_0}. \qquad \square \tag{C.4}$$

Proof of Property 2. Since $\boldsymbol{P}$ has full rank and $\boldsymbol{W}$ is positive definite, it can be concluded, using [20, 7.1.6, p. 399] that $\boldsymbol{G}=\boldsymbol{P}\boldsymbol{W}\boldsymbol{P}^T$ is symmetric and positive definite. The last part of the property states that $G^{-1}_{jk}=0$ for $k\notin N_j\wedge j\neq k$. This is proved using the fact that $\boldsymbol{P}^{-1}=\boldsymbol{A}$, hence $\boldsymbol{G}^{-1}=\boldsymbol{A}^T\boldsymbol{W}^{-1}\boldsymbol{A}$. The product is easily found since each column of $\boldsymbol{A}$ has no more than two non-zero elements. Denoting the initial nodes of l_j and l_k by m_p and m_q, respectively, the inverse matrix can be written as

$$G^{-1}_{jk}=\frac{1}{\mu_j}\delta_{jk}-\frac{1}{\mu_p}\delta_{pk}-\frac{1}{\mu_j}\delta_{jq}+\frac{1}{\mu_p}\delta_{pq}, \tag{C.5}$$

assuming that $m_p\neq m_0$ and $m_q\neq m_0$. The first term represents the diagonal of $\boldsymbol{G}^{-1}$. The next terms include the entries of upper and lower neighbors of l_j in the path to the root. The last term represents the situation where l_j and l_k have a common upper neighbor. Hence only entries representing neighbors of l_j are different from zero in the jth column of $\boldsymbol{G}^{-1}$. Similar calculations show that the property is also valid in case $m_p=m_0$ and/or $m_q=m_0$. $\square$

Proof of Property 3. First it is proved that $G_{jk}=M_{jk}-M_{jj}M_{kk}$, using the fact that the jth row of $\boldsymbol{P}$ can be expressed by means of the sub-tree T_j as in (4). By insertion it is seen that the first part of the product $\boldsymbol{G}=\boldsymbol{P}\boldsymbol{W}\boldsymbol{P}^T$ can be written

$$(PW)_{ji}=\sum_{k=1}^{n}P_{jk}W_{ki}=-\sum_{k\in T_j}\mu_k\delta_{ik}+\sum_{k\in T_j}\mu_k\mu_i=-\mu_i d_{ij}+\mu_i M_{jj}, \tag{C.6}$$

where $d_{ij}=1$ if $i\in T_j$, and zero otherwise. The elements of $\boldsymbol{G}$ are then found,

$$G_{jk}=\sum_{i=1}^{n}(PW)_{ji}P_{ki}=-M_{jj}\sum_{i\in T_k}\mu_i+\sum_{i\in T_k}\mu_i d_{ij}=M_{ij}-M_{ii}M_{jj}, \tag{C.7}$$

hence (25) is proved. The sum of the nodes in a sub-tree T_j is not affected by the reduction, which together with (25) proves the property. $\square$

Proof of Property 4. Denote again the nodes incident to l_j by m_j and m_p, and assume that $m_p\neq m_0$. The elements of $\boldsymbol{G}^{-1}$ are given in (C.5), which is also valid for $\hat{\boldsymbol{G}}^{-1}$ using the node values of the reduced graph. If $G^{-1}_{jk}=0$ then $k\in N_j$ or equivalently, $j\in N_k$. This can only be changed by the reduction if there exists an edge $q\in J$ such that $q\in N_j$ and $q\in N_J$. This implies that $j\in N_J$ and $k\in N_k$, which is in contradiction to the assumption, hence the property holds for $G^{-1}_{jk}=0$. The entry $G^{-1}_{jk}\neq 0$ if $j=k$ or $k\in N_j$ (equivalent $j\in N_k$). This neighboring relation cannot be changed by the reduction since $j,k\notin J$. The quantity G^{-1}_{jk} only depends on μ_j and μ_p, which will only change by the reduction if there exists an edge $q\in J$ incident to m_j or m_p. This means that $q\in N_j$ and consequently $j\in N_J$, which is again in contradiction to the assumption. Hence the property is proved for $m_p\neq m_0$. A similar argument can be made for $m_p=m_0$. $\square$

References

[1] M.L. Cosmo, E.C. Lorenzini (Eds.), Tethers in Space Handbook, NASA Marshall Space Flight Center, third ed., 1997.
[2] E.C. Lorenzini, M. Cosmo, S. Vetrella, A. Moccia, Dynamics and control of the tether elevator/crawler system, Journal of Guidance, Control, and Dynamics 12 (3) (1989) 404–411.
[3] S.S. Cohen, A.K. Misra, The effect of climber transit on the space elevator dynamics, Acta Astronautica 64 (5–6) (2009) 538–553, doi:10.1016/j.actaastro.2008.10.003.
[4] N. Takeichi, M. Natori, N. Okuizumi, Dynamic behavior of a tethered system with multiple subsatellites in elliptic orbits, Journal of Spacecraft and Rockets 38 (6) (2001) 914–921.
[5] C. Bombardelli, E.C. Lorenzini, M.B. Quadrelli, Retargeting dynamics of a linear tethered interferometer, Journal of Guidance, Control, and Dynamics 27 (6) (2004) 1061–1067.
[6] Y. Yang, B. HeXi, L. JunFeng, Dynamic modelling and analysis of space webs, Science China—Physics Mechanics & Astronomy 54 (4) (2011) 783–791, doi:10.1007/s11433-011-4290-4.
[7] P. Janhunen, Status report of the electric sail in 2009, Acta Astronautica 68 (2011) 567–570.
[8] A.K. Misra, V.J. Modi, Three-dimensional dynamics and control of tether-connected N-body systems, Acta Astronautica 26 (2) (1992) 77–84.
[9] A.D. Guerman, Equilibria of multibody chain in orbit plane, Journal of Guidance, Control, and Dynamics 26 (6) (2003) 942–948.
[10] V.V. Beletsky, E.M. Levin, Stability of a ring of connected satellites, Acta Astronautica 12 (10) (1985) 765–769.
[11] A. Pizarro-Chong, A.K. Misra, Dynamics of multi-tethered satellite formations containing a parent body, Acta Astronautica 63 (11–12) (2008) 1188–1202, doi:10.1016/j.actaastro.2008.06.021.
[12] J. Zhao, Z. Cai, Nonlinear dynamics and simulation of multi-tethered satellite formations in Halo orbits, Acta Astronautica 63 (5–6) (2008) 673–681, doi:10.1016/j.actaastro.2008.04.007.

Please cite this article as: M.B. Larsen, et al., Modeling of tethered satellite formations using graph theory, Acta Astronautica (2011), doi:10.1016/j.actaastro.2011.05.014

[13] S.G. Tragesser, A. Tuncay, Orbital design of earth-oriented tethered satellite formations, Journal of the Astronautical Sciences 53 (1) (2005) 51–64.
[14] A.K. Misra, Z. Amier, V.J. Modi, Attitude dynamics of three-body tethered systems, Acta Astronautica 17 (10) (1988) 1059–1068.
[15] A.D. Guerman, G. Smirnov, P. Paglione, A.M.V. Seabra, Stationary configurations of a tetrahedral tethered satellite formation, Journal of Guidance, Control, and Dynamics 31 (2) (2008) 424–428, doi:10.2514/1.31979.
[16] M. Keshmiri, A.K. Misra, V.J. Modi, General formulation for N-body tethered satellite system dynamics, Journal of Guidance, Control, and Dynamics 19 (1) (1996) 75–83.
[17] A. Guerman, Spatial equilibria of multibody chain in a circular orbit, Acta Astronautica 58 (1) (2006) 1–14, doi:10.1016/j.actaastro.2005.05.002.
[18] S.G. Tragesser, Static formations using momentum exchange between satellites, Journal of Guidance, Control, and Dynamics 32 (4) (2009) 1277–1286, doi:10.2514/1.40939.
[19] W.K. Chen, Graph theory and its engineering applications, Advanced Series in Electrical and Computer Engineering, vol. 5, World Scientific, 1996.
[20] R.A. Horn, C.R. Johnson, Matrix Analysis, Cambridge University Press, Cambridge, 1990 ISBN 0-521-38632-2, Corrected reprint of the 1985 original.

Please cite this article as: M.B. Larsen, et al., Modeling of tethered satellite formations using graph theory, Acta Astronautica (2011), doi:10.1016/j.actaastro.2011.05.014